Songklanakarin J. Sci. Technol.
41 (5), 992-998, Sep. - Oct. 2019

http://www.sjst.psu.ac.th

Original Article

Fourier transform infrared spectroscopy and elastic properties of $Mg_{1-x}Cd_xFe_2O_4$ ferrite systems

Satyappa Laxman Galagali[1], Rahul Annasaheb Patil[2], Raju Basappa Adaki[2], Chidanandayya Shivayya Hiremath[2], Shridhar Narasinhmurthy Mathad[3*], Appanna Shetteppa Pujar[1], and Rangappa Basappa Pujar[2]

[1] *Department of Physics, K.L.E. Society's Raja Lakhamagouda Science Institute, Belagaum, Karnataka, 590001 India*

[2] *Department of Physics, P.C. Jabin Science College, Hubballi, Karnataka, 580031 India*

[3] *Department of Physics, K.L.E. Institute of Technology, Hubli, Karnataka, 580030 India*

Received: 19 June 2017; Revised: 19 February 2018; Accepted: 28 May 2018

Abstract

Cadmium substituted magnesium ferrites were synthesized by a low-cost solid-state method. The cubic structure in homogenous state was realized by X-ray diffraction analysis. The Fourier transform infrared spectra of the films exhibited two absorption bands which illustrated the formation of the ferrite phase. The force constants for tetrahedral and octahedral sites were determined. The composition dependent changes in Young's modulus, rigidity modulus, bulk modulus, micro-strain, Debye temperature, dislocation density, transverse wave velocity, and longitudinal wave velocity were noticed. A Williamson-Hall plot and texture analysis studies of the samples were also conducted.

Keywords: ferrites, XRD, FTIR, texture coefficient, elastic properties

1. Introduction

Ferrites have a broad practical application in technology, due to the electrical and magnetic properties. Ferrites are technologically substantive materials that are used in the fabrication of electronic, microwave, and magnetic devices (Goldman, 2006). Ferrites are a class of oxides with remarkable magnetic properties and have been under investigation for five decades. Their applications encompass an impressive range extending from millimeter wave integrated circuitry to power handling, for instance, simple permanent magnets, transformer cores, antenna rods, memory chips, high-density magnetic recording media, transducers, activators, memory-devices, and computer components. Ferrites are widely used in drug delivery systems, microwave devices, and hyperthermia for cancer treatment (Challa, Kumar, & Faruq Mohammad, 2011; Snelling, 1969; Soohoo, 1960; Valenzuela, 2001). These applications are based on the basic properties of ferrites which are significant saturation magnetization, high electrical resistivity, low electrical losses, and very good chemical stability.

The soft magnetic Mg-ferrite ($MgFe_2O_4$) is an n-type semiconducting material, which possesses numerous attractive attributes such as high catalytic activity, high magnetic permeability, and humidity and gas sensing. Mg-ferrite has high resistivity, high Curie temperature, and it is environmentally stable which makes it a most worthy candidate for an extensive range of applications (Deraz, Omar, & Abd-Elkader, 2013). It was observed that cadmium (Cd^{+2}) doped Mg-ferrites were attractive due to increased saturation magnetization, magnetic moment, remanent magnetization, and coercive force. Cd^{+2} is a non-magnetic divalent ion which occupies essentially tetrahedral A-site when substituted in ferrites (Ashok *et al.*, 2012). Coercivity and saturation magnetization

*Corresponding author
Email address: physicssiddu@gmail.com

exhibits particle size dependent behavior. The reduction in the grain size compared to un-doped samples improves the magnetic properties. The dc resistivity decreases with temperature and increases with Cd^{+2} content. These values are higher than those obtained from the ceramic method (Gadkari, Shinde, & Vasambekar, 2013).

Several ferrites are being studied and processed by various techniques such as co-precipitation method, sol–gel combustion, modified oxidation process, forced hydrolysis, hydrothermal process, ball-milling, aerosol method, and the solid state method (Batoo & Ansari, 2012; Hanh, Quy, Thuy, Tung, & Spinu, 2003; Maria, Choudhury, & Hakim, 2013; Patil, Rendale, Mathad, & Pujar, 2015; Yattinahalli, Kapatkar, Ayachit & Mathad, 2013). Since no reports are available in the literature on the elastic properties of Mg-Cd ferrites, the present communication is an attempt to synthesize $Mg_{1-x}Cd_xFe_2O_4$ (where x = 0.2, 0.4, 0.6, and 0.8) by the simple solid state method. We investigated the influence of Cd^{+2} substitution on the structural and elastic properties of magnesium ferrites. We systematically report for the first time the influences of Cd^{+2} substitution in lattice constant (a), texture coefficient TC(hkl), and elastic properties of Mg-ferrite.

2. Experimental Techniques

Mg-Cd ferrites with the stoichiometric formula, Mg_{1-x} Cd_x Fe_2O_4 (where x = 0.2, 0.4, 0.6, and 0.8) were synthesized by the low cost solid state method. The compositional weights of the powders were mixed physically and blended in an agate mortar in an acetone medium. All samples were pre-sintered at 800 °C for 10 h keeping them in separate alumina crucibles in a muffle furnace. The pre-sintered powders were subjected to a hard milling process in acetone medium for a few hours. The pellets were then subjected to final sintering by keeping them on an alumina plate separately at 1000 °C for 15 h and the furnace was then cooled at the rate of about 80 °C/h. The schematic flowchart of the aim of the work is shown in Figure 1. The ferrites were subjected to X-ray diffraction on a PHILIPS-PW-3710 diffractometer with Cu-K□-radiation (□= 1.542A°). IR-absorption spectra were recorded between the wavenumbers of 300 and 1000 cm^{-1} on a Perkin Elmer (Spectrum-2000) Fourier transform infrared (FTIR) spectrophotometer.

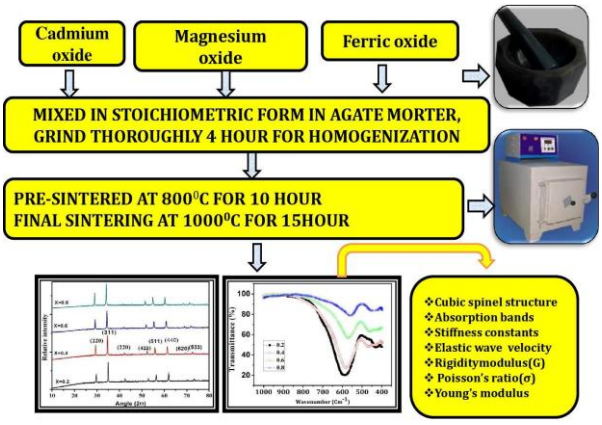

Figure 1. Block diagram of cadmium substituted Mg-ferrites.

3. Result Analysis

3.1 Structural studies

Figure 2 shows the X-ray diffraction patterns of the Mg-Cd ferrites. The main reflection planes are exhibited at 220, 311, 400, 422, 511, 333, and 440. In general, the diffraction patterns confirmed that the prepared samples crystallized into a cubic structure without any impurity phase (JCPDC card #00-001-0114). The broadening of the 311 peak was noticeable in the diffraction patterns of all samples which indicated the nano-size nature of the samples. The crystallite size is a measure of the size of a coherently diffracting domain. The average crystallite size for the different compositions was calculated by the Debye -Sherrer's formula (Mathad & Puri, 2014):

$$D = \frac{0.9 \cdot \lambda}{\beta . \cos\theta} \tag{1}$$

where, β is the full width at half length of maxima and λ is the wavelength of X-ray radiation. The crystallite size lies in the range of 41-56 nm. In accordance with Vegard's law, the lattice parameter (a) increased from 8.526 to 8.7499Å as the Cd^{+2} content (x) increased. The increase in the lattice parameter with Cd^{+2} doping was due to the larger ionic radius of Cd^{2+} (1.03 A^0) compared to Mg^{2+} (0.78A^0). The overall increase in the unit cell volume was due to the increase in the cell parameter (lattice parameter) of approximately 0.0262 to 0.0808%. The grain growth follows a regular trend with Cd^{+2} content, which is attributed to larger atomic weight of Cd^{+2} that favors grain growth. The lattice strain and average crystalline size were calculated using the Williamson-Hall equation (Kulkarni & Mathad, 2017):

$$\beta_{hkl} \cos\theta = \frac{K \cdot \lambda}{D} + 4\varepsilon \sin\theta \tag{2}$$

where ε is the lattice strain, D is the average crystallite size, λ is the wavelength of X-ray used, β is the full width half maximum, and θ is Bragg's angle. The graph of βcosθ versus sinθ is shown in Figure 3 and lattice strain (ε) was found in the range 0.288 to 1.238 and the crystallite size was found in

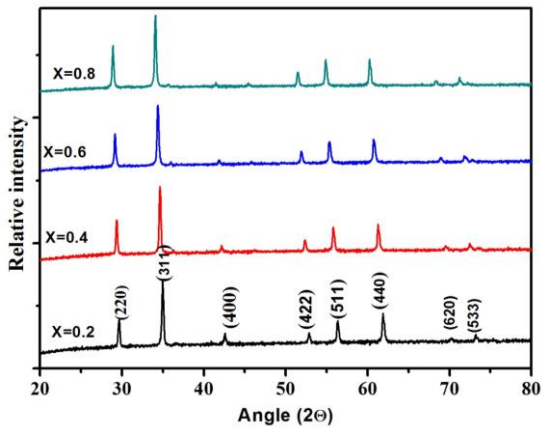

Figure 2. X-ray diffractgrams of ferrites.

the range 10-19 nm. Figure 4 shows the spherical shape of the micro-crystallites of the Mg-Cd ferrites observed with scanning electron microscopy. It is noticeable that the grain size increases as the Cd^{+2} doping increases and the average particle sizes are in the range of 0.38–0.80 µm. The grain size of x = 0.2 is 0.38 µm and x = 0.8 is 0.80 µm. Since every particle is

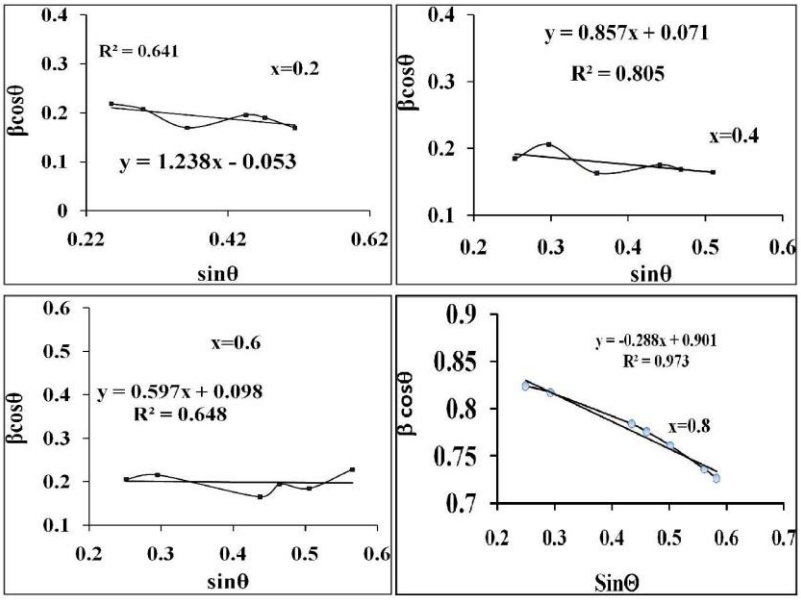

Figure 3. Williamson-Hall plot of Mg-Cd ferrites.

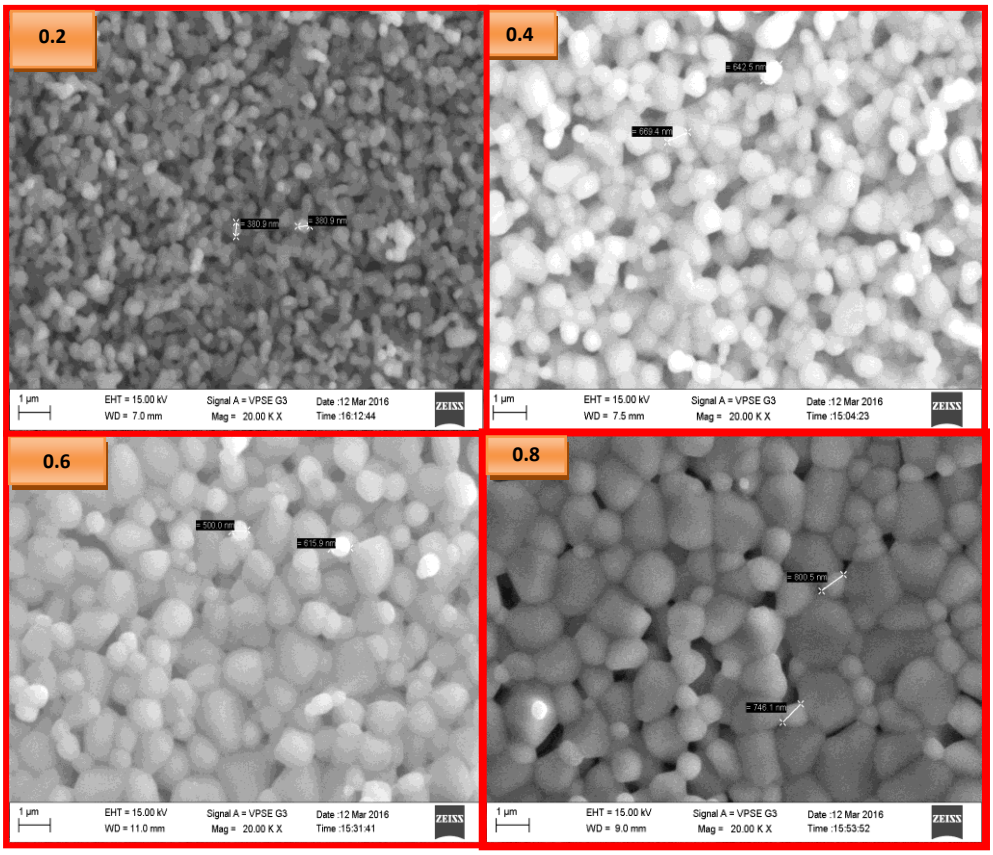

Figure 4. Scanning electron microscopy images of Mg-Cd ferrites.

aggregation of a number of crystallites or grains, the grain formed by the sizes are relatively larger than estimated by the Scherer formula due to instrument errors that were not taken into account. It is observed that the average grain size increases with the increase in Cd^{2+} content. This increase in grain size with increasing Cd^{2+} content is due to higher mobility of Cd^{2+} ions induced in the liquid phase sintering (Rezlescu, Sachelarie, Popa, & Rezlescu, 2000). This means grain growth follows a regular trend with Cd^{+2} content. This is attributed to the larger atomic weight of Cd^{+2} that favors grain growth (Gadkari, Shinde, & Vasambekar, 2010).

3.2 Texture analysis

XRD patterns indicate the presence of random orientation of crystallites, which have predictable relative peak intensities. Quantitative data concerning the preferential crystal orientation were calculated from the texture coefficient (TC) defined as

$$TC(hkl) = \frac{\frac{I(hkl)}{I_0(hkl)}}{\frac{1}{N}\sum_N \frac{I(hkl)}{I_0(hkl)}} \quad (3)$$

where I (hkl) is the measured intensity, I_0 (hkl) is the ASTM intensity and N is the reflection number. The texture analysis enunciates the physical and mechanical properties of the material. The texture in the polycrystalline samples signified the distinct spatial orientation of the individual crystallites within the material (Mathad & Puri, 2013). The lack of grain orientation in these planes (0<TC(hkl)<1) indicated the lack of grains oriented in that direction. The preferential orientation of the 311 plane found the abundance of grains increased as the Cd^{+2} content (TC[hkl]=2.6598).The abundance grain growth also found for the 440 plane for the sample x=0.8. It was observed that preferential orientation (abundance of grains) in all planes of Cd^{+2} content is tabulated in Table 1.

Table 1. Texture coefficients TC for significant (hkl) planes.

Planes (hkl)	Texture coefficient TC(hkl)			
	x=0.2	x=0.4	x=0.6	x=0.8
220	0.7866	0.7899	0.4504	0.2255
311	0.8989	0.9829	0.5785	2.6598
400	0.7495	1.5154	0.3125	0.1776
422	1.2069	0.7763	0.2118	0.1941
511	1.0401	0.8775	0.4679	2.7431
440	1.3178	1.057	3.9788	1.8616

3.3 Vibrational studies (FTIR studies)

Figure 5 shows the FTIR absorption bands of $Mg_{1-x}Cd_xFe_2O_4$ (with x=0.2, 0.4, 0.6, and 0.8) ferrite systems, which were recorded at room temperature in the wavenumber range of 400-1000 cm^{-1}. FTIR spectroscopy is a significant and non-destructive tool which furnishes qualitative information regarding structural details of crystalline materials. According to group theoretical considerations of Waldron (Waldron, 1955), there exist four fundamental I.R. active vibrational modes in the spinal structure. The first absorption band at the wavenumber ($\nu_1 \approx 600$ cm^{-1}) is attributed to the intrinsic vibrations of the tetrahedral complexes corresponding to the highest restoring force (Patil, Mahajan, Ghatage, & Lotke, 1998; Raju & Murthy, 2013; Shanmugavel, Gokul Raj, Rajarajan, & Ramesh Kumar, 2014; Shanmugavel, Gokul Raj, Rajarajan, Ramesh Kumar, & Boopathi, 2015).

The higher frequency absorption band (ν_1) is caused by scratching vibrations of the tetrahedral metal-oxygen bond and lower frequency absorption band (ν_2) is caused by metal-oxygen vibrations in octahedral sites (Gadkari *et al.*, 2010). The absorption band edges, tetrahedral (K_t) and octahedral sites (K_o) force constants of the samples are tabulated in Table 2. According to Waldron's method, the force constants are calculated using the following equations:

octahedral site force constant

$$(K_0) = 0.942128\ M_1\ \nu_2^2 / [M_A+32] \quad (4)$$

where M_A is the molecular weight on A-site;

tetrahedral site force constant

$$(K_t) = 0.04416\ M_B\ \nu_1^2 [V/V+3] \quad (5)$$

where M_B is themolecular weight on B-site.

$$V=[64 - (2\ M_A U)]/M_B \text{ and } U = 2K_o/(M_B\ \nu_1^2 - 2K_0) \quad (6)$$

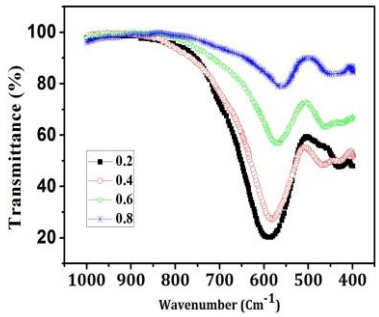

Figure 5. FTIR spectrogram of $Mg_{1-x}Cd_xFe_2O_4$ (x = 0.2, 0.4, 0.6, and 0.8) ferrites.

Table 2. Absorption band maxima and force constants.

Composition (x)	Absorption band edges (Wave number) in cm^{-1}		Force constants in dynes / cm	
	ν_1	ν_2	Kt $X10^5$	Ko $X10^5$
0.2	590	410	2.70	0.946
0.4	580	420	2.95	0.991
0.6	575	475	2.58	1.23
0.8	560	450	2.34	1.07

The bond lengths ($R_{A\text{-}O}$ and $R_{B\text{-}O}$) and ionic radii (r_A and r_B) on tetrahedral (A) and octahedral (B) sites are calculated using the relations (Yattinahalli, Kapatkar, & Mathad, 2014). The calculated values of bond lengths and ionic radii on *A*-site and *B*-site are depicted in Figure 6.

$$A-O=(u-1/4)a\sqrt{3} \quad (7)$$

$$B-O=(5/8-u)a \quad (8)$$

$$r_A=(u-1/4)a\sqrt{3}-r(O^{2-}) \quad (9)$$

$$r_B=(5/8-u)a-r(O^{2-}) \quad (10)$$

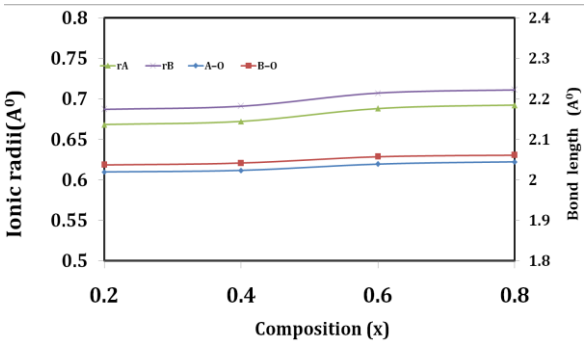

Figure 6. Variation of ionic radii and bond lengths with cadmium content (x).

It can be seen that the bond lengths (A–O, B–O) and ionic radii (r_A, r_B) increase with the increase in Cd^{+2} content in the system, which in turn causes the lattice constant to increase with the increase in Cd^{+2} content. It can be concluded that the tetrahedral substitution plays the dominant role in influencing the value of the lattice constant. The correlation between the ionic radius and lattice constant is well known. Composition dependence represents the bond lengths and cation radii in spinel ferrites which has been reported by various researchers (Kambale, Shaikh, Bhosale, Rajpure, & Kolekar, 2009; Raghasudha, Ravinder, & Veerasomaiah, 2013; Surender Kumar, Shinde, Vasambekar, 2013). The interatomic distances like tetrahedral bond length (d_{Ax}), octahedral bond length (d_{Bx}), shared tetragonal edge (d_{AEx}), shared octahedral edge (d_{BxE}) and unshared octahedral edge (d_{BxEu}) were calculated (Patil, Rendale, Mathad, & Pujar, 2017).

$$d_{Ax}=a(u-1/4)\sqrt{3} \quad (11)$$

$$d_{Bx}=a[3u^2-\frac{11}{4}u+\frac{43}{64}]^{1/2} \quad (12)$$

$$d_{AEx}=a(2u-\frac{1}{2})\sqrt{2} \quad (13)$$

$$d_{BxE}=a(1-2u)\sqrt{2} \quad (14)$$

$$d_{BxEu}=a\sqrt{[4u^2-3u+\frac{11}{16}]} \quad (15)$$

The variations in edge lengths & bond lengths as Cd^{+2} content changes were found to systematically increase linearly (Figure 7).

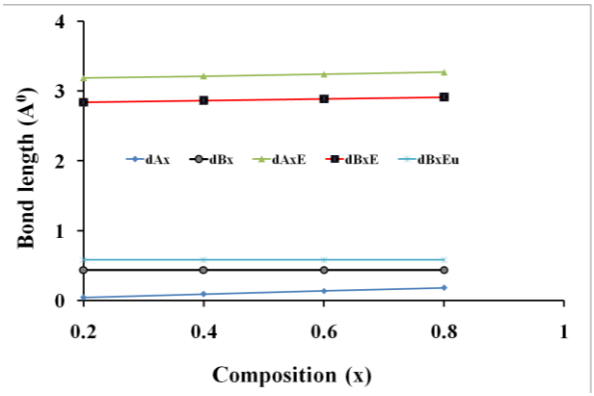

Figure 7. Variation of edge lengths with cadmium content (x).

3.4 Elastic properties

The study of elastic properties of ferrites is important in industry and is attributable to their extraordinary elastic behavior which determines the strength of the materials below versatile strained conditions. The elastic properties of ferrite systems were technically supported by FTIR spectrum analyses (Modi *et al.*, 2004). Debye temperature simplifies the integration of the heat capacity. The Debye temperature indicates the approximate temperature limit below which quantum effects may be observed. In Debye theory, the Debye temperature (Θ_D) is the temperature of a crystal's highest normal mode of vibration, i.e. the highest temperature that can be achieved due to a single normal vibration (Modi *et al.*, 2004). The stiffness constants (for an isotropic material, C_{11}=C_{12}), longitudinal elastic wave (V_l), the transverse elastic wave (V_t), mean elastic velocity (V_{Mean}), rigidity modulus (G), Poisson's ratio (σ), and Young's modulus (E) have been specified (Hill, 19 86) and tabulated in Table 3.

$$C_{11}=C_{12}=K_{av}/a \quad (16)$$

$$V_l=\{\frac{C_{11}}{dx}\}^{1/2} \quad (17)$$

$$V_t=\{V_l/\sqrt{3}\} \quad (18)$$

$$V_M=\left[V_i^3V_t^3\Big/V_t^3+2V_i^3\right]^{1/3} \quad (19)$$

$$G=dx.V_t^2 \quad (20)$$

$$B=\frac{1}{3}(C_{11}+2C_{12}) \quad (21)$$

$$P=\left[\frac{3B-2G}{6B+2G}\right] \quad (22)$$

$$E=2G(1+P) \quad (23)$$

$$\Theta_D=\frac{hcv_{av}}{2\pi k} \quad (24)$$

From Table 3, it can be understood that the B, E, and G for the Cd^{+2} content (x), are interpreted in terms of the inter-atomic bonding (Mazen & Elmosalami, 2011). The

Table 3. Stiffness constants, longitudinal elastic wave, transverse elastic wave, mean elastic velocity, rigidity modulus, Poisson's ratio, Young's modulus (E), and Debye temperature.

Composition (x)	Various parameters								
x	C_{11} GPa	B GPa	V_l m/s	V_t m/s	V_{mean} m/s	G GPa	P	E GPa	Θ K
x=0.2	213.88	213.88	6318.27	3647.85	3246.26	71.29	0.35	96.24	345.07
x=0.4	228.91	228.91	6540.37	3776.08	3360.26	76.3	0.35	10.30	345.07
x=0.6	219.71	219.71	6409.99	3700.81	3293.34	73.24	0.35	98.87	348.67
x=0.8	209.46	209.46	6259.97	3614.19	3216.33	69.82	0.35	94.25	345.79

variation of transverse, longitudinal, and mean velocities with Cd^{+2} content (x) is shown in Figure 8. The magnitude of the velocities are minimum for x=0.8. The magnitude of Poisson's ratio (σ) were found to be constant (σ=0.35) for all samples, which lies in the range from −1 to 0.5. These Poisson's ratio (σ) values were consistent with the theory of isotropic elasticity (Modi, Rangolia, Chhantbar, & Joshi, 2006). It was found that all elastic parameters and Debye temperature obtained from FTIR data were in good agreement with different ferrite systems. (Mazen & Elmosalami, 2011; Modi, Rangolia, Chhantbar, & Joshi, 2006; Patil, Rendale, Mathad, & Pujar, 2017; Yattina-halli *et al.*, 2014)

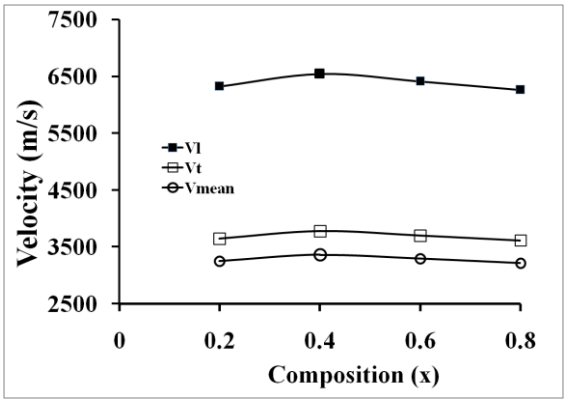

Figure 8. Variation of longitudinal velocity, transverse velocity, and mean velocity with cadmium variation.

4. Conclusions

In this paper, we have analogized the Cd^{+2} substituted Mg ferrites by a low cost, simple solid state method. It was found that the lattice parameter increased from 8.526 Å to 8.7499 Å as the Cd^{+2} concentration increased which obeyed Vegard's law. The Mg-Cd ferrite powder that was obtained was highly crystalline and free from any impurities with a crystallite size range of 41-56 nm. The increases in the unit cell volumes and cell parameters were approximately 0.0262 to 0.0808%. This grain growth followed the regular trend of Cd^{+2} content which was attributed to the larger atomic weight of Cd^{+2} that favors grain growth. The main absorption bands of spinel ferrite appeared through IR absorption spectra recorded in the range of 300-1000 cm^{-1}. The elastic properties of ferrites with Cd^{+2} were interpreted in terms of binding forces.

References

Ashok, A., Somaiah, T., Ravinde, D., Venkateshwarlu, C., Reddy, C. S., Rao, K. N., & Prasad, M. (2012). Electrical Properties of Cadmium Substitution in Nickel Ferrites. *World Journal of Condensed Matter Physics, 2*(4), 257-266. doi:10.4236/wjcmp.2012.24043

Aziliz, H., & Nguyen Thị Kim, T. (2014). Magnetic nanoparticle-based therapeutic agents for thermo-chemotherapy treatment of cancer. *Nanoscale*, *6*, 11553-11573. doi:10.1039/C4NR03482A

Batoo, K. M., & Ansari, M. S. (2012). Low temperature-fired Ni-Cu-Zn ferrite nanoparticles through auto-combustion method for multilayer chip inductor applications. *Nanoscale Research Letters*, *7*(1). doi:10.1186/ 1556-276X-7-112

Challa, S. S., Kumar, R., & Faruq, M. (2011). Magnetic Nanomaterials for Hyperthermia-based Therapy and Controlled Drug Delivery. *Advanced Drug Delivery Reviews*, *63*(9), 789–808. doi:10.1016/j.addr.2011.03.008

Deraz, N. M., & Abd-Elkader, O. H. (2013). Effects of Magnesia Content on Spinel Magnesium Ferrite Formation. *International Journal of Electrochemical Science*, *8*, 8632–8644.

Gadkari, A. B., Shinde, T. J., & Vasambekar, P. N. (2010). Structural and magnetic properties of nanocrystalline Mg–Cd ferrites prepared by oxalate co-precipitation method. *Journal of Materials Science Materials in Electronics*, *21*, 96–103. doi:10.1007/s10854-009-9875-6

Gadkari, A. B., Shinde. T. J., & Vasambekar, P. N. (2013). Influence of rare earth ion (Y^{3+}) on the magnetic and dc electrical properties of high density nanocrystalline MgCd ferrites. *Materials Research Bulletin*, *48* (2), 476-481. doi:10.1016/j.materresbull.2012.11.009

Goldman, A. (2006). *Modern ferrite technology*, *2nd edition.* New York, NY: Springer.

Hanh, N., Quy, O. K., Thuy, N. P., Tung, L. D., & Spinu, L. (2003). Synthesis of cobalt ferrite nanocrystallites by forced hydrolysis and investigation of their magnetic properties. *Physica B*, *327*, 382–384, doi:10.1016/S0921-4526(02)01750-7

Hill, T. L. (1986). *An introduction to statistical thermodynamics*. New York, NY: Dover Publications.

Kambale, R. C., Shaikh, P. A., Bhosale, C. H., Rajpure, K. Y., & Kolekar, Y. D. (2009). Dielectric properties and complex impedance spectroscopy studies of mixed Ni–Co ferrites. *Smart Materials and Structures, 18* (8), 085014. doi:10.1088/0964-1726/18/8/085014

Kazi, M., Shamima, C., & Hakim, M. A. (2013). Structural phase transformation and hysteresis behavior of Cu-Zn ferrites. *International Nano Letters*, *3*, 42. doi: 10.1186/2228-5326-3-42

Kulkarni, A. B., & Mathad, S. N. (2018). Synthesis and structural analysis of Co-Zn-Cd ferrite by Williamson-Hall and Size-Strain Plot Methods. *International Journal of Self-Propagating High-Temperature Synthesis*, *27*(1), 37–43. doi:10.3103/S106138621801003X

Kumar, S., Shinde, T. J., & Vasambekar, P. N. (2013). Microwave synthesis and characterization of nanocrystalline Mn-Zn ferrites. *Advanced Materials Lett*ers, *4* (5), 373-377. doi:10.5185/amlett.2012.10429

Mathad, S. N., & Puri, V. (2014). Microwave Studies of Environmental Friendly Ferroelectrics. *International Scholarly Research Notices.* doi:10.1155/2014/683986

Mazen, S. A., & Elmosalami, T. A. (2011). Structural and Elastic Properties of Li-Ni Ferrite. *ISRN Condensed Matter Physics*. doi:10.5402/2011/820726

Mod, K. B. (2004). Elastic moduli determination through IR spectroscopy for zinc substituted copper ferri chromates. *Journal of Materials Science*, *39*(8), 2887–2890.

Modi, K. B., Rangolia, M. K., Chhantbar, M. C., & Joshi, H. H. (2006). Study of infrared spectroscopy and elastic properties of fine and coarse grained nickel-cadmium ferrites. *Journal of Materials Science, 41* (22), 7308–7318. doi:10.1007/s10853-006-0929-3

Modi, K. B., Trivedi, U. N., Pandya, M. P., Bhatu, S. S., Chhantba, M. C., & Joshi, H. H. (2004). Microwaves and Optoelectronics, New Delhi, India: Anamaya Publishers.

Patil, M. R., Rendale, M. K., Mathad, S. N., & Pujar, R. B. (2015). Structural and IR study of $Ni_{0.5-x}Cd_xZn_{0.5}Fe_2O_4$. *International Journal of Self-Propagating High-Temperature Synthesis, 24*(4), 241–245. doi:10.3103/S1061386215040081

Patil, M. R., Rendale, M. K., Mathad, S. N., & Pujar, R. B. (2017). FTIR spectra and elastic properties of Cd-substituted Ni–Zn ferrites. *International Journal of Self Propagating High-Temperature*, *26*(1), 33–39. doi:10.3103/S1061386217010083

Patil, S. A., Mahajan, V. C., Ghatage, A. K., & Lotke, S. D. (1998). *Materials Chemistry and Physics*, 57, 86-92.

Raghasudha, M. D., & Ravinder, P. V. (2013). Characterization of nano-structured magnesium chromium ferrites synthesized by citrate-gel auto combustion method. *Advanced Materials Lett*ers, *4*(12), 910-916. doi:10.5185/amlett.2013.5479

Raju, P., & Murthy, S. R. (2013). Microwave-hydrothermal synthesis of $CoFe_2O_4$-TiO_2 nano-composites. *Advanced Materials Lett*ers, 4(1), 99-105. doi:10.5185/amlett.2013.icnano.130

Rezlescu, E., Sachelarie, L., Popa, P. D., & Rezlescu, N. (2000). Effect of Substitution of Divalent Ions on the Electrical and Magnetic Properties of Ni–Zn–Me Ferrites. *IEEE Transactions on Magnetics, 36*(6), S 0018-9464(00)10065-2. doi:10.1109/20.914348

Shanmugavel, T. S., Gokul, R. S., Rajarajan, G., & Ramesh, K. (2014). Rapid phase synthesis of nanocrystalline cobalt ferrite. *AIP Conference Proceedings 1591 496*(2014). doi:10.1063/1.4872651

Shanmugavel, T., Gokul, R. S., Rajarajan, G., Ramesh, K., & Boopathi, G. (2015). Combustion synthesis and structural analysis of nanocrystalline nickel ferrite at low temperature regime. *AIP Conference Proceedings 1665 050182*(2015). doi:10.1063/1.4917823

Snelling, E. C. (1969). *Soft Ferrites: Properties and Application*. London, England: ILIFFE Books.

Soohoo, R. F. (1960). *Theory and Application of Ferrites*. Englewood Cliffs, NJ: Prentice-Hall.

Valenzuela, R. (2012). Novel Applications of Ferrites. *Hindawi Publishing Corporation Physics Research International*, 1-9. doi:10.1155/2012/591839

Waldron, R. D. (1955). Infrared spectra of ferrites. *Physical Review*, *99*(6), 1727–1765. doi:10.1103/PhysRev.99.1727

Yattinahalli, S. S., Kapatkar, S. B., & Mathad, S. N. (2014). Structural and mechanical properties of a nanoferrite. *Advanced Science Focus, 2*(2), 42–46.

Yattinahalli, S. S., Kapatkar, S. B., Ayachit, N. H., & Mathad, S. N. (2013). Synthesis and Structural Characterization of Nano-sized Nickel Ferrite. *International Journal of Self-Propagating High Temperature Synthesis, 22*(3), 147–150. doi:10.3103/S1061386213030114